



**HAL**  
open science

# Adsorption of acetonitrile ( $\text{CH}_3\text{CN}$ ) on Si ( 111 ) – 7 x 7 at room temperature studied by synchrotron radiation core-level spectroscopies and excited-state density functional theory calculations

F. Bournel, S. Carniato, G. Dufour, J.-J. Gallet, V. Ilakovac, S. Rangan, F. Rochet, F. Sirotti

## ► To cite this version:

F. Bournel, S. Carniato, G. Dufour, J.-J. Gallet, V. Ilakovac, et al.. Adsorption of acetonitrile (  $\text{CH}_3\text{CN}$  ) on Si ( 111 ) – 7 x 7 at room temperature studied by synchrotron radiation core-level spectroscopies and excited-state density functional theory calculations. *Physical Review B*, 2006, 73 (12), pp.125345. 10.1103/PhysRevB.73.125345 . hal-03966776

**HAL Id: hal-03966776**

**<https://hal.science/hal-03966776>**

Submitted on 16 Feb 2023

**HAL** is a multi-disciplinary open access archive for the deposit and dissemination of scientific research documents, whether they are published or not. The documents may come from teaching and research institutions in France or abroad, or from public or private research centers.

L'archive ouverte pluridisciplinaire **HAL**, est destinée au dépôt et à la diffusion de documents scientifiques de niveau recherche, publiés ou non, émanant des établissements d'enseignement et de recherche français ou étrangers, des laboratoires publics ou privés.

# Adsorption of acetonitrile ( $\text{CH}_3\text{CN}$ ) on $\text{Si}(111)\text{-}7\times 7$ at room temperature studied by synchrotron radiation core-level spectroscopies and excited-state density functional theory calculations

F. Bournel, S. Carniato,\* G. Dufour, J.-J. Gallet, V. Ilakovac, S. Rangan,<sup>†</sup> and F. Rochet<sup>‡</sup>  
*Laboratoire de Chimie Physique Matière et Rayonnement, Université Pierre et Marie Curie, 11 rue Pierre et Marie Curie, 75231 Paris Cedex 05, France*

F. Sirotti

*Synchrotron SOLEIL, L'Orme des Merisiers Saint-Aubin, Boîte Postale 48, 91192 Gif sur Yvette Cedex, France*

(Received 19 December 2005; published 29 March 2006)

The room temperature adsorption of acetonitrile ( $\text{CH}_3\text{-C}\equiv\text{N}$ ) on  $\text{Si}(111)\text{-}7\times 7$  is examined by synchrotron radiation  $\text{N } 1s$  x-ray photoemission and x-ray absorption spectroscopies. The experimental spectroscopic data point to multiple adsorption geometries. Candidate structures are optimized using density functional theory (DFT), the surface being simulated by silicon clusters encompassing one (adjacent) adatom–rest atom pair. This is followed by the DFT calculation of electron transition energies and cross sections. The comparison of theoretical spectra with experimental ones indicates that the molecule is adsorbed on the surface under two forms, a nondissociated geometry (an  $sp^2$ -hybridized CN) and a dissociated one (leading to a pendent  $sp$ -hybridized CN). In the nondissociative mode, the molecule bridges an adatom–rest atom pair. For bridge-type models, the discussion of the core-excited state calculations is focussed on the so-called silicon-molecule mixed-state transitions that strongly depend on the breaking or not of the adatom backbonds and on the attachment of the nitrogen end either to the adatom or to the rest atom. Concerning the dissociated state, the CH bond cleavage leads to a cyanomethyl ( $\text{Si-CH}_2\text{-CN}$ ) plus a silicon monohydride, which accounts for the spectroscopic evidence of a free  $\text{C}\equiv\text{N}$  group (we do not find at 300 K any spectroscopic evidence for a  $\text{C}\equiv\text{N}$  group datively bonded to a silicon atom via its nitrogen lone pair). Therefore the reaction products of acetonitrile on  $\text{Si}(111)\text{-}7\times 7$  are similar to those detected on the  $\text{Si}(001)\text{-}2\times 1$  surface at the same temperature, despite the marked differences in the reconstruction of those two surfaces, especially the distance between adjacent silicon broken bonds. In that respect, we discuss how adatom backbond breaking in the course of adsorption may explain why both surface orientations react the same way with acetonitrile.

DOI: [10.1103/PhysRevB.73.125345](https://doi.org/10.1103/PhysRevB.73.125345)

PACS number(s): 68.43.Fg, 68.47.Fg, 71.15.Mb, 61.10.Ht

## I. INTRODUCTION

The reactivity of molecules toward clean reconstructed silicon surfaces is clearly correlated with the presence of surface dangling bonds. In the case of the  $\text{Si}(001)\text{-}2\times 1$  surface, the buckling of the silicon dimer leads to only two kinds of triply coordinated atoms, the “electron-rich” outer dimer atom and the “electron-poor” inner dimer atom.<sup>1</sup> On the other hand, in the case of the  $\text{Si}(111)\text{-}7\times 7$  surface, the dimer–adatom–stacking fault (DAS) reconstruction<sup>2</sup> (Fig. 1) results in a much more complex situation, as there exist a variety of inequivalent triply coordinated Si bearing a dangling bond. The 19 broken bonds of the unit cell are borne by 12 adatoms (ADs), six rest atoms (RAs), and one corner hole atom. Charge transfer between adatoms and rest atoms provides an additional mechanism for lowering the energy. The six rest atoms plus the corner hole atom are able to convert their half-filled dangling bond into a more stable lone pair by extracting seven electrons from the 12 adatoms. In a band picture, one would have a set of metallic adatoms bands (with a  $5/12$  filling) crossing the Fermi level, plus a completely filled rest atom band. This picture is valid at least at room temperature, as confirmed by an angle-resolved photoemission mapping of the Fermi surface.<sup>3</sup> While the adatom bands show dispersion in the reciprocal space, the small

band dispersion of the rest atoms states point to their localized nature. The local viewpoint provided by scanning tunneling microscopy (STM) and scanning tunneling spectroscopy<sup>4–6</sup> is in accord with the overall picture given by valence band photoemission<sup>3</sup> and inverse photoemission.<sup>7</sup> Naturally STM imagery gives detailed information on the charge density at the various sites. In particular the electronic structure of the unfaulted and faulted triangular subunits composing the  $7\times 7$  cell are not equivalent. The faulted subunit has a higher electron charge density than the unfaulted one,<sup>6</sup> with obvious consequences on chemical reactivity. Moreover, the center and corner adatom dangling bonds in both subunits have also different heights relative to the rest plane,<sup>8–10</sup> likely in relation to a different filling of their dangling bonds. Therefore, in contrast to the case of the buckled  $\text{Si}(001)\text{-}2\times 1$  surface, a simple Lewis picture of the  $\text{Si}(111)\text{-}7\times 7$  surface broken bonds in terms of basic (the closed shell rest atoms) and acidic sites (the partially filled adatoms dangling bonds) may be not fully adequate: the key issue is the charge transfer reversibility between those two sites, first suggested by Avouris and Wolkow in their STM study of ammonia adsorption.<sup>4</sup> The ammonia molecule (which bears a lone pair) would react counterintuitively with an electron-rich rest atom, the excess charge being transferred to the neighboring adatoms. In the framework of the

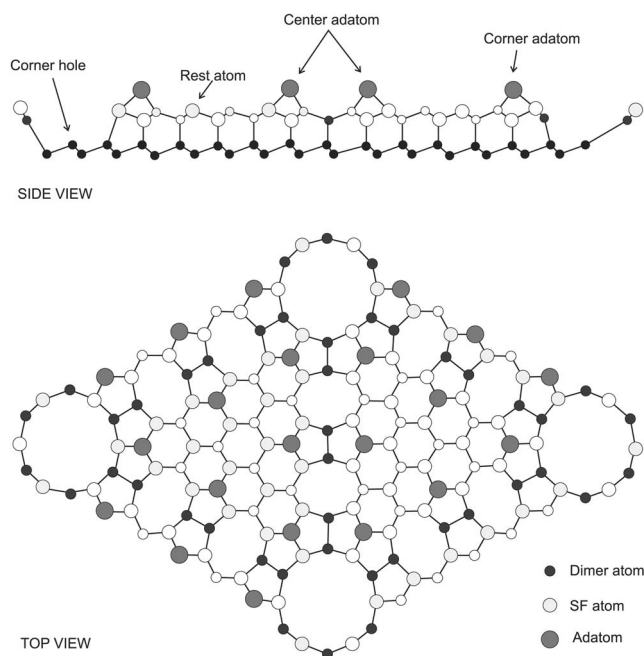


FIG. 1. Schematic diagram illustrating the DAS model (Ref. 2) of the  $7 \times 7$  surface reconstruction. SF stacking fault.

density functional theory (DFT), a cluster<sup>11</sup> calculation and a periodic slab calculation<sup>12</sup> (using a simplified  $4 \times 2$  surface unit cell) have been performed recently: the former (latter) supports (invalidates) the “charge transfer” model.

In recent years, many surface science studies have been devoted to the reactivity of organic molecules toward silicon surfaces, because their functionalization is promising in view of potential electronic applications.<sup>13</sup> Paralleling studies carried out on the “technological” Si(001) surface,<sup>1,14</sup>  $\pi$ -bonded molecules, such as acetylene<sup>15–17</sup> and ethylene,<sup>18–20</sup> have been adsorbed on the Si(111)- $7 \times 7$  surface. One expects that the  $\pi$  bond opens to form a so-called di- $\sigma$  bonding with two surface silicon broken bonds. For acetylene and ethylene, the experimental data are consistent with such a picture, and the bridging of a rest atom–adatom pair—despite the large ( $\sim 4.5$  Å) distance separating these two atoms—is generally envisaged, at least at relatively low coverage; see, e.g., Refs. 16, 17, 19, and 20. More recently, the reactivity of the cyano group ( $-\text{C}\equiv\text{N}$ ) in acetonitrile,<sup>21,22</sup> allylcyanide,<sup>23</sup> and benzonitrile,<sup>24</sup> has also been investigated on the Si(111) surface. The study of this functionality is indeed particularly interesting. Being isoelectronic to  $-\text{C}\equiv\text{C}-$ , acetonitrile is also expected to undergo an  $sp$ -to- $sp^2$  rehybridization over a pair of dangling bonds. Naturally, adjacent rest atom–adatom pairs can be those sites. Various bridging geometries are depicted in Figs. 2(a)–2(e). Bearing a lone pair on its nitrogen, a dative bonding with a silicon dangling bond also deserves consideration. In the latter case the reaction site should be an adatom dangling bond (empty or partially filled). However, the attachment of the nitrogen end on a rest atom might be steered by the transfer of the excess charge to the neighboring adatoms. Two possible dative bonding geometries are sketched in Figs. 2(f) and 2(g). Note that dative bonding geometries could be precursor states to the bridging geometries of Figs. 2(a)–2(d).

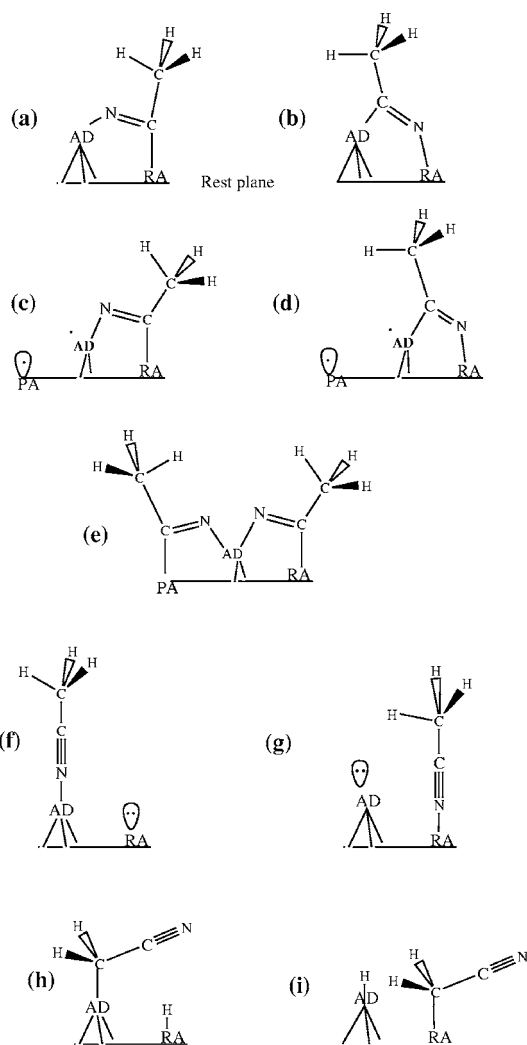


FIG. 2. Possible adsorption modes of acetonitrile on Si(111)- $7 \times 7$  (AD=adatom, RA=rest atom, PA=pedestal atom). (a)  $\text{bridge}_{\text{N-AD}}$ , (b)  $\text{bridge}_{\text{N-RA}}$ , (c)  $\text{bridge}_{\text{N-AD}}$  plus broken PA–AD bond, (d)  $\text{bridge}_{\text{N-RA}}$  plus broken PA–AD bond, (e) double bridge, (f) AD dative, (g) RA dative, (h) AD–cyanomethyl plus RA–H, and (i) RA–cyanomethyl plus AD–H.

The preceding works<sup>21,22</sup> devoted to acetonitrile adsorption on the Si(111)- $7 \times 7$  surface have been carried out essentially at cryogenic temperature. In the STM work of Shirota *et al.*<sup>21</sup> carried out at 120 K the molecular image is not seen directly. The presence of the molecule is only inferred from changes in the apparent height of the adatoms involved in the reaction. The lack of visible molecular imprints on this surface is a general fact of observation, that is likely related to the too localized nature of the silicon electron states which have a limited overlap with the molecular orbitals of the adsorbate.<sup>25</sup> The adsorption site would consist in two center adatoms situated on each side of the dimer line dividing the faulted and unfaulted subunits. The observation of reacted adatoms does not enable by itself a precise characterization of the adsorbate chemical bonding. On the other hand, the high-resolution electron energy loss spectroscopy (HREELS) study of Feng Tao *et al.*<sup>22</sup>—carried out at 110 K—is clearly indicative of an  $sp$ -to- $sp^2$  rehybridization of the  $\text{C}\equiv\text{N}$  moi-

ety (there is no indication of molecular dissociation). Valence band photoemission shows also that adatoms and rest atoms are involved in the chemical bonding. Therefore Tao and co-workers conclude that the molecule likely bridges a rest atom–adatom pair, as sketched in Figs. 2(a) and 2(b). The interpretation of the low-temperature STM image made in Ref. 21 is difficult to reconcile with the HREELS detection of a bridge bonding. As a matter of fact, the distance separating center adatoms across the dimer row is 6.65 Å, a value which seems too large to enable the formation of a Si–C≡N–Si unit, as the distance between two silicon pairs should be less than 5.1 Å (1.98+1.29+1.80 Å). Note that the characteristic vibrational signature of a C≡N moiety is also observed for the other nitriles.<sup>23,24</sup>

The only available study on acetonitrile adsorption at room temperature is a STM imaging of the surface by Tao and co-workers.<sup>22</sup> Images point to a change in the electron occupancy of adatoms, revealed by a change in their brightness: reacted adatoms darken. Statistically, the faulted subunits are more reactive than the unfaulted ones and center adatoms are more reactive than corner adatoms, a situation reminiscent of the case of ethylene adsorption.<sup>19</sup> After a 0.2 L exposure, ca. 27% of the adatoms are reacted. At saturation (the dose is not indicated), the percentage of reacted adatoms reaches 42%. Then their number per triangular subunit is about 3, that is the number of rest atoms. According to Tao and co-workers, this observation lends strong support to the rest atom–adatom bridging geometry at 300 K.

Tao and co-workers<sup>22</sup> have also calculated the adsorption energy of a molecule adopting a bridge geometry. They use a simplified model of the actual surface, a Si<sub>9</sub>H<sub>12</sub> cluster representing a rest atom–adatom pair. Their DFT calculations lead to adsorption energies of –1.06 eV for the bridge<sub>N–AD</sub> model [Fig. 2(a)] and of –1.19 eV for the bridge<sub>N–RA</sub> model [Fig. 2(b)]. The authors do not discuss the fact that the adatom may be dragged away from its initial position by the bridging molecule.

In the analogous case of acetylene adsorption over a rest atom–adatom pair, the DFT calculation of Lu *et al.*<sup>26</sup> using a Si<sub>16</sub>H<sub>18</sub> cluster shows that the rest atom–adatom distance is reduced from 4.4 to 3.5 Å. In their recent semiempirical calculation—a slab containing two 7×7 unit cells is used—Sbraccia *et al.*<sup>27</sup> find two equilibrium geometries for acetylene bridging the AD–RA gap, one conserving an intact bond between the pedestal atom (PA) and the AD, and one for which this bond is broken. The latter geometry is found to be the more stable. However, when the same authors perform a periodic DFT calculation—then they use a reduced 2×2 surface cell—they find that the bridging geometry with a broken PA–AD bond is the only stable one. Therefore, for acetonitrile also, the issue of PA–AD bond breaking in bridging geometries must be addressed: such geometries are sketched in Figs. 2(c) and 2(d). Note that the breaking of the PA–AD bond could also leave enough room for the bridging of a second molecule, in a “double bridge geometry,” as sketched in Fig. 2(e).

In their calculation Tao and co-workers<sup>22</sup> have not addressed the issue of molecular dissociation. In fact our recent x-ray absorption study on the adsorption of acetonitrile on Si(001)-2×1 points to the breaking of the C–H bond over a

dimer and the subsequent formation of a cyanomethyl (Si–CH<sub>2</sub>–C≡N) plus a silicon monohydride.<sup>28</sup> This results from the acidic nature of the αH atom.<sup>29</sup> Over a rest atom–adatom pair the C–H bond could also break [note that H<sub>2</sub>O (Refs. 30 and 31) and NH<sub>3</sub> (Refs. 4 and 32) dissociate both over a Si<sub>2</sub> dimer of the Si(001) surface and over a rest atom–adatom pair of the Si(111)-7×7 surface]. Two types of cyanomethyls could form on the surface, the AD-cyanomethyl on an adatom [Fig. 2(h)] or the RA-cyanomethyl on a rest atom [Fig. 2(i)].

The goal of the present study is the determination of the electronic structure of acetonitrile adsorbed at room temperature on Si(111)-7×7, by combining N 1s core-level photoemission and near-edge x-ray absorption fine structure (NEXAFS) spectroscopies to DFT electron transition energy computation, following the approach of Refs. 28 and 33. It is shown that synchrotron radiation spectroscopies give valuable information on the various bondings of acetonitrile on Si(111)-7×7, especially in a context in which a direct and detailed image of the adsorption geometry cannot be provided by STM topographic scans.

## II. EXPERIMENT

The Si(111) substrates (phosphorus doped, 0.003 Ω cm resistivity) were cleaned from their native oxide by flashing at 1250 °C, and then cooled down to room temperature before exposure to the gas. The surface reconstruction was checked by low-energy electron diffraction and its cleanliness by Si 2*p* photoemission (see Sec. IV). Acetonitrile which is liquid at room temperature was contained in a glass vial and purified by repeated “freeze-pump-thaw” cycles. The molecule was introduced directly in the analysis chamber via a leak valve. The gas purity was controlled with a quadrupole mass analyzer.

Electron spectroscopy measurements were performed at the SB7 beamline of the SuperACO storage ring (LURE synchrotron facility, Orsay, France), using a Dragon type monochromator at a bending magnet.<sup>34</sup> The source was linearly polarized (95%), the main component of the electric field (**E**) being contained in the horizontal plane. The sample could rotate around a vertical axis, so that the beam incidence angle  $\theta$  (measured with respect to the sample surface plane) could be changed.  $\theta$  is also equal to the angle between **E** and the normal to the surface (see Fig. 3).

X-ray photoelectron spectroscopy (XPS) was carried out using a “Scienta 200” hemispherical analyzer. Si 2*p* core-level spectra were measured at a photon energy of 145 eV to obtain conditions of maximum surface sensitivity (for photoelectrons of kinetic energy about 45 eV an escape depth of about 3.5 Å is estimated<sup>35</sup>). N 1s XPS spectra were measured at  $h\nu=440$  eV. Binding energies are referenced with respect to the Fermi level. Therefore the Si 2*p*<sub>3/2</sub> binding energy of the clean surface is at 99.45 eV.

NEXAFS N 1s spectra were taken in the Auger yield mode (N KVV transitions) to achieve a good adsorbate sensitivity (for further details see Ref. 28). The spectra were normalized with respect to the secondary electron photoemission peak dominated by contributions from bulk Si. The

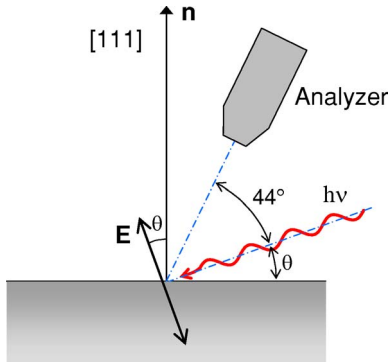


FIG. 3. (Color online) Geometry of the experiment. The x rays are incident in the horizontal orbit plane of the storage ring, which contains the major electric field component  $\mathbf{E}$  (the polarization factor being 95%, the weaker component is orthogonal to the orbit plane).  $\mathbf{n}$  is the surface normal, parallel to  $[111]$ . The x-ray incidence angle  $\theta$ , which is also the polar angle of  $\mathbf{E}$ , is changed by rotating the silicon crystal about the axis of the (vertical) manipulator.  $\theta$  can be set at any value between  $16^\circ$  (grazing incidence) and  $90^\circ$  (normal incidence). The axis of the electron analyzer makes an angle of  $44^\circ$  with the beam direction.

photon bandwidth was about 200 meV. The photon energy was calibrated using the first- and second-order light from the monochromator. We measured the angular dependence of the NEXAFS absorption intensity with the light incidence angle  $\theta$ , between  $90^\circ$  (normal incidence) and  $16^\circ$  (grazing incidence). Indeed, dichroic spectra give valuable information on the adsorption geometries. Due to the dipolar selection rules,  $K$ -edge NEXAFS probes the unfilled states of  $p$  symmetry. The absorption has a characteristic  $\cos^2(\delta)$  dependence, where  $\delta$  is the angle between the  $p$  orbital axis and the polarization vector  $\mathbf{E}$  of the synchrotron radiation.<sup>36</sup> Therefore the direction of bonds having a characteristic symmetry ( $\sigma, \pi$ ) can be inferred from the experimental dichroic absorption spectra, and adsorption models can be validated or eliminated.

### III. COMPUTATIONS

#### A. DFT cluster calculation of the adsorption geometries

Optimized adsorption geometries are calculated with the GAMESS(US) software package<sup>37</sup> using Becke3 Lee-Yang-Parr (B3LYP) three-parameter DFT theory.

Because of the size and complexity of the DAS unit cell, our DFT calculation is based on a simplified model of the actual surface structure. Two types of clusters have been used to represent the adjacent adatom-rest atom pair on a faulted half of a  $\text{Si}(111)\text{-}7\times 7$  surface unit cell. The  $\text{Si}_{16}\text{H}_{18}$  cluster and the  $\text{Si}_{21}\text{H}_{24}$  cluster are depicted in Figs. 4(a) and 4(b), respectively. Then the molecule is added to each type of “mother” cluster.

With  $\text{Si}_{16}\text{H}_{18}$ , the geometrical optimization of the adduct is made using a  $6\text{-}311\text{G}^*$  basis set for nitrogen, carbon, and silicon atoms. The H ligands are described by a  $6\text{-}31\text{G}^*$  basis. With  $\text{Si}_{21}\text{H}_{24}$ , due to the large cluster size, we use a (SBKJc+1d) basis set for all silicon atoms and a  $6\text{-}311\text{G}^*$

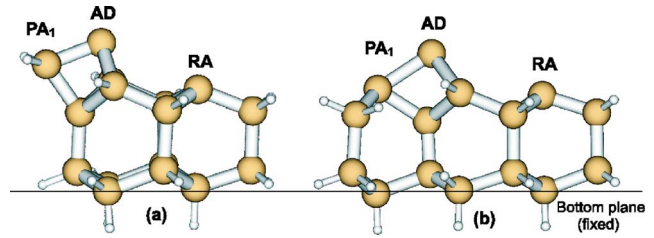


FIG. 4. (a) (Color online) The  $\text{Si}_{16}\text{H}_{18}$  cluster. (b) The  $\text{Si}_{21}\text{H}_{24}$  cluster. In both cases, the (111) plane is defined by the bottom layer of Si atoms kept at bulk positions.

basis set for the nitrogen, carbon, and hydrogen atoms. In all geometry optimizations, the bottom layer Si atoms are kept fixed at bulk lattice positions, so defining the “(111) surface plane.” All the other Si atoms and their H terminations are free to relax.

The  $\text{Si}_{16}\text{H}_{18}$  cluster had been used previously in theoretical investigations of the chemisorption of ammonia<sup>11</sup> and of various  $\pi$  bonded molecules on  $\text{Si}(111)$ .<sup>26</sup> The advantage of this cluster is its relatively small size: the main problem encountered in the present simulation is the convergence of core-excited states within a large system, given the large basis sets we use (see below). Its drawback is the “flexibility” of the rest plane due to the fact that the pedestal atom denoted  $\text{PA}_1$  in Fig. 4(a) is connected to two H atoms instead of two silicon atoms of the second layer. For bridging geometries such as those depicted in Figs. 2(a)–2(c) the adatom is dragged toward the rest atom, without breaking the  $\text{PA}_1$ -AD bond (see below and Ref. 26). Kang<sup>12</sup> and Sbraccia *et al.*<sup>27</sup> consider that the distortion of the rest plane is non-physical and leads to spurious effects in the calculation of adsorption geometries and reaction paths. Therefore a more realistic representation of the surface should make use of a stiffer restplane. However it is clear that for nonbridging geometries such as the dissociated models of Figs. 2(h) and 2(i), the rest plane flexibility is no longer a problem and that the  $\text{Si}_{16}\text{H}_{18}$  cluster is convenient in the latter case.

In the  $\text{Si}_{21}\text{H}_{24}$  cluster,  $\text{PA}_1$  is now topologically connected to the bottom (fourth layer) Si atom via three six-membered silicon rings (as in the real surface). This ensures the stiffness of the restplane atoms, when the bottom plane Si are fixed to their bulk position. Consequently, the stable bridging configurations we find (see Sec. IV) are of the “broken adatom backbond” type [Figs. 2(c) and 2(d)]. Thus the use of the  $\text{Si}_{21}\text{H}_{24}$  cluster gives us the opportunity to examine the influence of the broken  $\text{PA}_1$ -AD bond on the electronic structure of the bridge adduct, by comparison with the similar structures calculated with the  $\text{Si}_{16}\text{H}_{18}$  cluster.

#### B. Core-excited states

The local minima geometries we find for the molecule plus Si cluster system are the starting point of the calculation of NEXAFS transitions and ionization potentials (IP). (Note that in the calculation the IP is the binding energy measured from the vacuum level, while experimentally the binding energies are referenced with respect to the Fermi level.) The quantum chemical *ab initio* calculations of the N 1s excited

states are performed at a DFT level of theory. The application of DFT to core-photoionization phenomena takes advantage that both the relaxation and correlation effects are simultaneously described at a moderate computational cost, with respect to self-consistent field SCF and post-HF methods. We used a modified version of the GAMESS(US) program, enabling (i) the choice of a fractional occupancy for the core-hole and (ii) the calculation of singlet core-excited energy values.<sup>38</sup> We used an IGLOO-III basis set<sup>39</sup> for the nitrogen atom along with a special diffuse  $[3s, 3p, 3d]$  basis added at the core-ionized or -excited site.

### 1. Absolute NEXAFS transitions and IPs calculated via the $\Delta$ Kohn-Sham method

Absolute values of NEXAFS transitions are calculated via the so-called  $\Delta$ Kohn-Sham method (denoted hereafter  $\Delta$ KS). The energy of the core excited state is calculated by removing one electron from the  $1s$  and adding one to the empty orbital of interest. Then the transition energy is obtained as the difference between the energy of the excited state and that of the ground state. The relativistic correction of 0.3 eV is included, according to Triguero *et al.*<sup>40</sup> The  $\Delta$ KS triplet final state transition energies are corrected using the sum method of Ziegler, Rauk, and Baerends,<sup>41</sup> to account for the spin conservation in dipolar transitions leading to a singlet final state.

For the calculation of N  $1s$  ionization potentials, the same  $\Delta$ KS method is applied, IP being the difference between the energy of the excited state, represented by a core hole in the  $1s$  orbital, and that of the ground state.

The accuracy of the  $\Delta$ KS method is excellent for the isolated acetonitrile molecule, for which we obtain a calculated NEXAFS  $\pi_{C\equiv N}^*$  transition of 399.9 eV and an IP of 405.6 eV, to be compared with the experimental gas phase  $\pi_{C\equiv N}^*$  transition found at  $399.9 \pm 0.1$  eV,<sup>42</sup> and the experimental gas phase IP of 405.6 eV.<sup>43</sup>

Note that the influence of the silicon cluster size on N  $1s$  NEXAFS and IP calculated transitions has been examined in the case of the acetonitrile/Si(001) (Ref. 28) and benzonitrile/Si(001) (Ref. 33) systems. Increasing the cluster size has no effect on the NEXAFS transitions calculated with the  $\Delta$ KS method. On the other hand, the IP energy typically diminishes by 0.2–0.3 eV when the cluster size is multiplied by a factor of about 2 (from a  $Si_9H_{12}$  single-dimer cluster to a  $Si_{21}H_{20}$  three-dimer cluster). This may be understood in terms of final-state contribution. For a NEXAFS transition the core-hole is screened by the excited electron, and the “substrate” screening plays a limited role. For an ionic state, the screening contribution of the “substrate” is large and the cluster size matters.

### 2. NEXAFS cross-section calculation within the single-electron approach

X-ray absorption cross sections are calculated by use of the single-electron core and virtual (excited-state) orbitals, within the dipolar approximation (it is assumed that the radiation is linearly polarized). We have tested various approaches aiming at taking into account the relaxation

effects in the NEXAFS state. The electron occupancy of the  $1s$  core level, of the lowest unoccupied molecular orbital (LUMO) and of virtual orbitals higher in energy than the LUMO ( $LUMO+n$ ), can be chosen in various ways. As the variational principle can be applied to densities referring to any state with fractional occupancy, we have examined (i) the transition potential approach ( $1s^{1/2}$  final state),<sup>28,44</sup> (ii) the  $(1s)^1(LUMO)^1$  model,<sup>33,44</sup> and finally (iii) the  $(1s)^1(LUMO)^{1/2}(LUMO+1)^{1/2}$  model. In this type of approach, the transition energy is the difference between the energy of the virtual orbital and that of the  $1s$  orbital. In the present work, we have adopted the  $(1s)^1(LUMO)^{1/2}(LUMO+1)^{1/2}$  method which gives the most accurate *relative* NEXAFS transition energies with respect to those calculated with the  $\Delta$ KS method. As the *absolute* values of the transition energies may be 0.5–1 eV off the experimental ones, the NEXAFS spectra are repositioned on an absolute energy scale provided by the energy of the first (lower  $h\nu$ ) bound excited state calculated with the  $\Delta$ KS method.

In isolated molecules, a step is seen experimentally at the IP,<sup>45</sup> due to the transition to the free-electron continuum. In the present calculation, we have considered that the adspecies plus Si cluster can be considered as a molecule, having discrete bound states below the IP and discrete states embedded in the energy continuum of the free electron above the IP. Below the IP, the NEXAFS spectrum consists of the discrete lines calculated by the  $(1s)^1(LUMO)^{1/2}(LUMO+1)^{1/2}$  method and broadened by convolution with a Gaussian of 0.6 eV full width at half maximum (FWHM). For transitions calculated above the IP, we convert the discrete lines into a continuum using the Stieltjes imaging procedure,<sup>46</sup> (the calculated continuum cross section is convoluted with the same Gaussian function used for the discrete part below IP).

## IV. RESULTS AND DISCUSSION

### A. Experimental spectra

We begin this section by examining how the surface states of the Si  $2p$  core-level line “feels” the adsorption of the acetonitrile molecule at room temperature (Fig. 5). The clean surface Si  $2p$  spectrum is characterized by a surface state shifted by ca.  $-0.80$  eV from the silicon bulk line. This state is attributed to the restatoms.<sup>47</sup> From STM imagery it is known that adatoms react at 300 K.<sup>22</sup> Si  $2p$  XPS proves that rest atoms are also involved in the chemical reaction: for an acetonitrile dose of  $10^{-8}$  mbar  $\times$  600 s, i.e., 4.5 L, one sees that the rest atom line intensity is strongly diminished. An exposure to a larger dose ( $10^{-7}$  mbar  $\times$  600 s, i.e., 45 L) does not modify appreciably the spectral shape. The formation of new bonds (Si–C or Si–N) cannot be inferred with the present resolution (the bulk Si  $2p_{3/2}$  line has a FWHM of 0.5 eV). Figure 5 shows also the absence of band curvature shift upon molecule adsorption. Despite surface states are consumed during absorption, the Fermi level pinning within the semiconductor gap is not affected.

The N  $1s$  photoemission spectrum of the Si(111)- $7 \times 7$  surface exposed to acetonitrile under a pressure of  $10^{-7}$  mbar

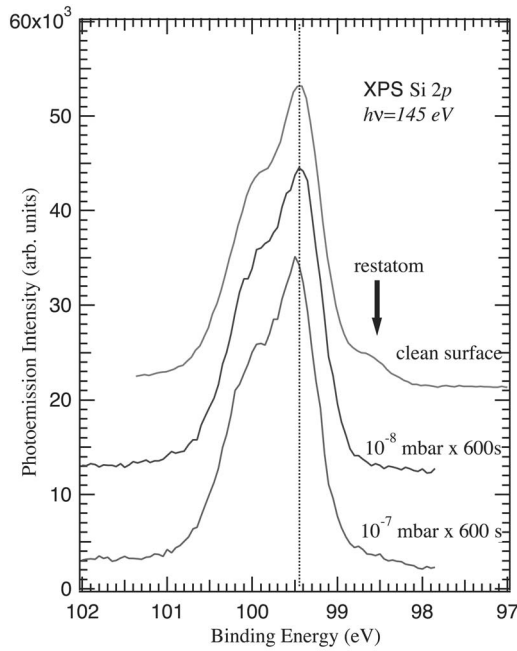


FIG. 5. Raw experimental Si 2*p* core level of a Si(111)-7×7 surface exposed to increasing doses of acetonitrile at room temperature. The spectra are measured at normal electron emergence.

for 600 s (Fig. 6) exhibits two structures peaked at 397.60 and 398.95 eV, respectively, in a 48:52 proportion. This is indicative of the presence of (at least) two different chemical environment for the nitrogen atom.

The corresponding NEXAFS N 1*s* curves, given in Fig. 7, present two  $\pi^*$  transitions. The first one appears at 397.65 eV. Its intensity decreases from normal to grazing incidence, suggesting the nitrogen *p* lobes are rather parallel to the silicon surface. The second transition is seen at 399.80 eV and its intensity varies little with  $\theta$ .

**B. Spectra simulation**

**1. Choice of the models**

At this stage of the discussion, a comparison with the case of acetonitrile adsorbed on Si(001)-2×1 at 300 K is

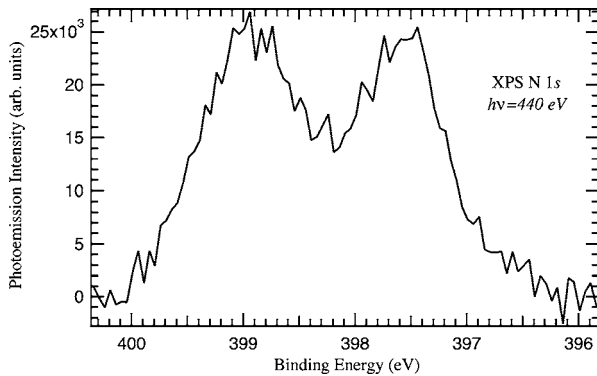


FIG. 6. Experimental N 1*s* core level of the Si(111)-7×7 surface exposed to an acetonitrile dose of 10<sup>-7</sup> mbar×600 s at 300 K. The spectrum is measured at an electron emergence of 30° with respect to the surface normal. The background has been subtracted. The attribution of the spectral lines is given in Table IV.

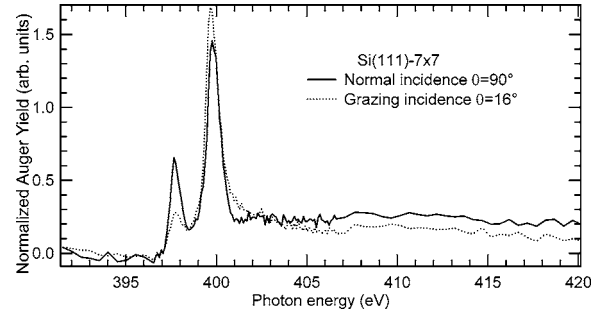


FIG. 7. Experimental normalized N 1*s* NEXAFS spectra of the Si(111)-7×7 surface exposed to an acetonitrile dose of 10<sup>-7</sup> mbar×600 s at 300 K. The measurements are made under grazing ( $\theta=16^\circ$ , that is, **E** nearly perpendicular to the surface plane) and normal incidence ( $\theta=90^\circ$ , that is, **E** contained in the surface plane). The attribution of the various spectral lines is given in Table IV.

helpful.<sup>28</sup> In the acetonitrile/Si(001) system, two main NEXAFS transitions (see Figs. 6 and 7 of Ref. 28) are observed experimentally at 397.7 and 399.8 eV, that is, at the same photon energies as those seen in the case of the acetonitrile/Si(111) system. The confrontation of experimental data to DFT calculations, lead us to attribute the transition at 397.65 eV to a “side-on” adsorption mode (a Si–C=N–Si unit) and the one at 399.8 eV to a pendent C≡N (interpreted as a cyanomethyl Si–CH<sub>2</sub>–C≡N). A third line, observed at 399 eV for CH<sub>3</sub>CN on Si(001), was attributed to a  $\sigma^*$ (Si–N bond) transition (denoted hereafter  $\sigma_{\text{Si-N}}^*$ ) of the side-on geometry. The absence of such a line at ca. 399 eV in the NEXAFS spectra of the acetonitrile/Si(111) system (see Fig. 7), which will be discussed in Sec. IV C, does not alter the general picture we are suggesting.

Guided by analogies with the acetonitrile-Si(001) system, we have examined here adsorption geometries that lead to the formation of double and triple CN bonds, in the context of the (111)-7×7 reconstruction. Our N 1*s* NEXAFS simulation has been limited to the Si–C=N–Si bridge and cyanomethyl plus Si–H geometries involving a rest atom–adatom pair. The NEXAFS spectra of acetonitrile datively bonded to an adatom or a rest atom have not been calculated, although the corresponding NEXAFS transition should also be found around 400 eV [the calculation gives 400.3 eV for acetonitrile datively bonded on the Si(001)-2×1 surface<sup>28</sup>]. Indeed, in such a case, the  $\pi$  system should be contained in the surface plane. The nondichroic behavior of the transition at 399.8 eV makes the presence of a dative bonding at 300 K very unlikely (see also Sec. IV C).

TABLE I. Calculated distances for the cluster optimized geometries. PA<sub>2</sub> is a pedestal atom out of the mirror plane defined by PA<sub>1</sub>, AD, and RA atoms. Distances are given in angstroms.

Cluster type	Si <sub>16</sub> H <sub>18</sub>	Si <sub>21</sub> H <sub>24</sub>
d <sub>AD-RA</sub>	4.34	4.50
d <sub>AD-PA<sub>1</sub></sub>	2.38	2.44
d <sub>AD-PA<sub>2</sub></sub>	2.37	2.40

TABLE II. Calculated distances and angles for the optimized AD-RA bridge geometries.  $\gamma$  is the angle between the normal to the (111) plane and the Si-N bond axis. Distances are given in angstroms and angles in degrees.

Cluster type model	Si <sub>16</sub> H <sub>18</sub>	Si <sub>21</sub> H <sub>24</sub>
	bridge <sub>N-AD</sub> /bridge <sub>N-RA</sub>	bridge <sub>N-AD</sub> /bridge <sub>N-RA</sub>
$d_{AD-RA}$	3.38/3.53	3.60/3.56
$d_{AD-PA_1}$	2.41/2.43	3.97/3.90
$d_{Si-N}$	1.77/1.79	1.70/1.77
$d_{Si-C}$	2.00/1.99	1.95/1.98
$d_{C=N}$	1.28/1.27	1.27/1.26
$\angle SiNC$	120.5/137.4	149.2/143.3
$\gamma$	57.5/10.4	75.9/9.1

The calculated spectra are given for two x-ray light incidences, normal ( $\theta=90^\circ$ , i.e.,  $\mathbf{E}$  parallel to the surface; see Fig. 3) and grazing ( $\theta=20^\circ$ ,  $\mathbf{E}$  nearly orthogonal to the surface). The threefold symmetry of the Si(111) surface around the [111] axis is taken into account in the spectrum calculation. The outputs of geometrical optimizations (bond lengths, angles, etc.), that are useful for the discussion, are collected in Table I (before molecular attachment) and Table II (after formation of the AD-RA bridge geometries). In Table III, we give the  $\Delta$ KS NEXAFS transition energies and IPs corresponding to the various envisaged models.

## 2. AD-RA bridging geometries with a Si<sub>16</sub>H<sub>18</sub> cluster

When the molecule bridges the adatom–rest atom pair, the Si<sub>16</sub>H<sub>18</sub> cluster simulation shows that the adatom is dragged toward the rest atom as shown in the insets of Figs. 8 and 9 (refer also to Tables I and II). The rest atom–adatom distance is reduced from 4.34 to 3.38 Å (3.53 Å) for the “bridge<sub>N-AD</sub>” geometry (respectively for the “bridge<sub>N-RA</sub>” geometry). The PA<sub>1</sub>-adatom bond length is slightly stretched—from 2.38 to

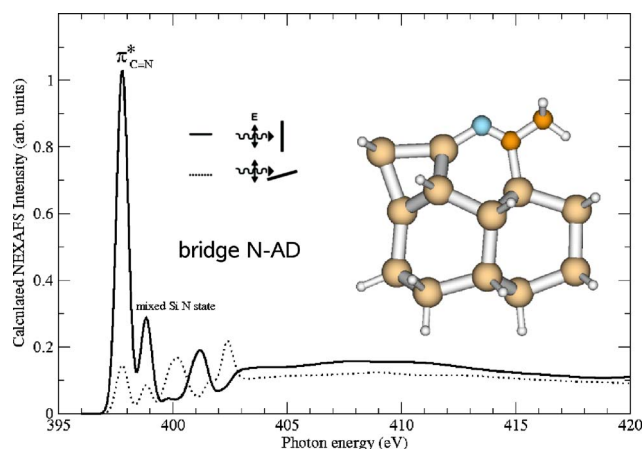


FIG. 8. (Color online) Simulated N 1s NEXAFS spectra of the bridge<sub>N-AD</sub> model (Si<sub>16</sub>H<sub>18</sub> cluster), for two orientations of the electric field (solid line,  $\theta=90^\circ$ ; dotted line,  $\theta=20^\circ$ ). The threefold substrate symmetry is taken into account. The IP is 403.0 eV. The corresponding optimized geometry is given in the inset.

2.41 Å (N-AD model) and 2.43 Å (N-RA model)—but it does not break. (Note that the same kind of distortion of the initial Si<sub>16</sub>H<sub>18</sub> cluster geometry was obtained by Lu *et al.* in the case of acetylene adsorption.<sup>26</sup>) The calculated CN bond length is 1.28 Å for the N-AD and 1.27 Å for the N-RA geometry, a value expected for  $sp^2$  hybridization. The  $\angle SiNC$  angle is  $120.54^\circ$  for the N-AD geometry and  $137.4^\circ$  for the N-RA geometry, closer in the former case to the ideal ( $120^\circ$ ) angle of  $sp^2$  bonding.

For both bridge models, the theoretical  $\pi_{C=N}^*$  transitions are close in energy, 397.8 eV for the N-AD model and 398.1 eV for the N-RA model. Our simulation (Figs. 8 and 9) shows also that this  $\pi_{C=N}^*$  transition, polarized in the (111) surface plane, is maximum at normal incidence and vanishing at grazing incidence. An examination of the so-called silicon-molecule mixed states is also worthy of interest. For the N-RA model, the line at 399 eV, strongly polar-

TABLE III. Calculated  $\Delta$ KS NEXAFS transitions and  $\Delta$ KS IPs for various models of the acetonitrile/Si(001) system. Energies are given in eV.

Model and cluster	Calculated NEXAFS transitions	Type and polarization	Calculated IP
Free molecule	399.9	$\pi_{C=N}^*$	405.6
Bridge <sub>N-AD</sub>	397.8	$\pi_{C=N}^*$ $\mathbf{E} // (111)$	403.0
Si <sub>16</sub> H <sub>18</sub>	399.1	Mixed state $\mathbf{E} // (111)$	
Bridge <sub>N-RA</sub>	398.1	$\pi_{C=N}^*$ $\mathbf{E} // (111)$	403.1
Si <sub>16</sub> H <sub>18</sub>	399.0	$\sigma_{Si-N}^*$ $\mathbf{E} \perp (111)$	
Bridge <sub>N-AD</sub>	397.6	$\pi_{AD=N}^*$ $\mathbf{E} \perp (111)$	403.3
Si <sub>21</sub> H <sub>24</sub>	398.0	$\pi_{C=N}^*$ $\mathbf{E} // (111)$	
Bridge <sub>N-RA</sub>	397.4	“N 2p + AD db” $\mathbf{E} \perp (111)$	403.0
	398.1	$\pi_{C=N}^*$ $\mathbf{E} // (111)$	
Si <sub>21</sub> H <sub>24</sub>	399.5 <sup>a</sup>	$\sigma_{Si-N}^*$ $\mathbf{E} \perp (111)$	
RA-cyanomethyl	399.8	$\pi_{C=N}^*$	404.7
Si <sub>16</sub> H <sub>18</sub>			

<sup>a</sup>Calculated by adding the  $(1s)^1(LUMO)^{1/2}(LUMO+1)^{1/2}$  model energy shift to the absolute  $\Delta$ KS value of the lower-energy transition

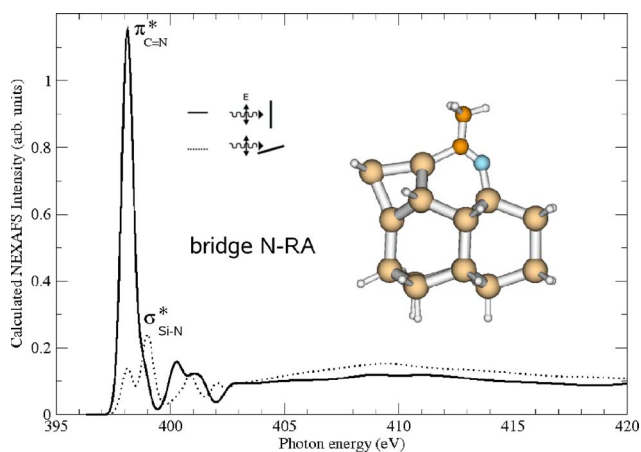


FIG. 9. (Color online) Simulated N 1s NEXAFS spectra of the bridge<sub>N-RA</sub> model (Si<sub>16</sub>H<sub>18</sub> cluster), for two orientations of the electric field (solid line,  $\theta=90^\circ$ ; dotted line,  $\theta=20^\circ$ ). The threefold substrate symmetry is taken into account. The IP is 403.1 eV. The corresponding optimized geometry is given in the inset.

ized perpendicularly to the (111) plane, has a clear  $\sigma_{\text{Si-N}}^*$  character, as shown in Fig. 10. Its dichroism stems from the fact that the Si-N axis makes an angle  $\gamma$  of  $10^\circ$  with the normal to the (111) plane. On the other hand, for the N-AD model, the mixed state calculated at about 399 eV—with a polarization parallel to the surface—does not exhibit a “revolution symmetry” around the Si-N bond axis.

### 3. AD-RA bridging geometries with a Si<sub>21</sub>H<sub>24</sub> cluster

We consider now the case of a bridge<sub>N-AD</sub> plus broken PA-AD bond geometry. The optimized geometry is shown in Figs. 11 and 12 (refer also to Table II). Before the attachment of the molecule, the Si<sub>21</sub>H<sub>24</sub> cluster exhibited a PA<sub>1</sub>-adatom distance of 2.44 Å, close to the one obtained for the Si<sub>16</sub>H<sub>18</sub>

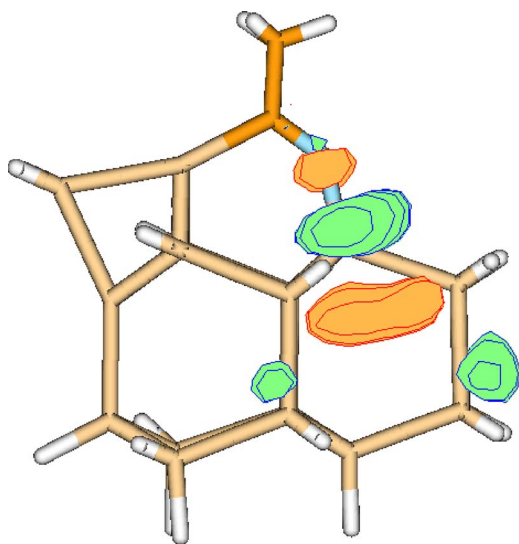


FIG. 10. (Color online) The  $\sigma_{\text{Si-N}}^*$  orbital of the unbroken adatom backbond bridge<sub>N-RA</sub> geometry [(1s)<sup>1</sup>(LUMO)<sup>1/2</sup>(LUMO+1)<sup>1/2</sup> state]. It gives rise to a NEXAFS transition at 399 eV; see Fig. 9.

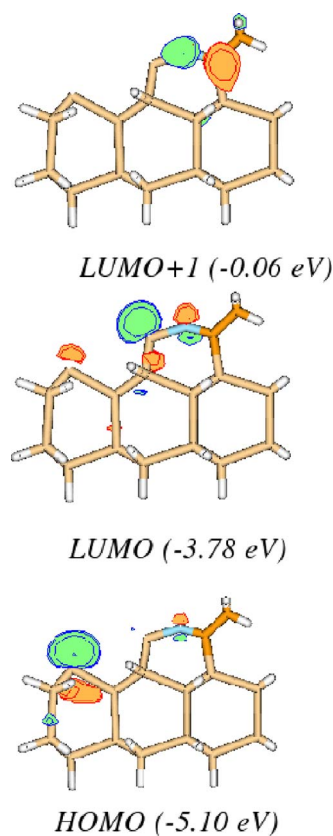


FIG. 11. (Color online) Ground state orbitals of the bridge<sub>N-AD</sub> plus broken PA-AD bond geometry: HOMO (PA<sub>1</sub> dangling bond), LUMO ( $\pi_{\text{AD=N}}^*$ ), LUMO+1 ( $\pi_{\text{C=N}}^*$ ). The corresponding energies are also given. To help comparison with the extended solid case, note that the work function (affinity) of the clean Si(111)-7 $\times$ 7 surface is  $\sim 4.65$  eV ( $\sim 4.16$  eV). (Ref. 48).

cluster (2.38 Å). But as soon as the molecule bridges the adatom-rest atom site, the large PA<sub>1</sub>-adatom distance (3.97 Å) we obtain indicates that the bond is broken. The rest atom-adatom distance imposed by molecular bridging is now 3.60 Å, slightly larger than that found for the “flexible” Si<sub>16</sub>H<sub>18</sub> cluster. The calculated CN bond length is 1.27 Å, a value expected for  $sp^2$  hybridization, but the  $\angle$ SiNC angle ( $149^\circ$ ) is larger than the ideal value of  $120^\circ$ . The AD-N bond axis makes an angle  $\gamma$  of about  $76^\circ$  with respect to the normal to the (111) plane. The Kohn-Sham orbitals calculated for the *ground state* are worth looking at (see Fig. 11). First the highest occupied molecular orbital (HOMO) is essentially concentrated on the PA<sub>1</sub> atom. This indicates that the scheme given in Fig. 2(c)—where both the PA<sub>1</sub> and AD broken bonds bear an unpaired electron—has to be somewhat revised, as the PA<sub>1</sub> dangling bond is filled by electron transfer from the adatom. Notice also that the LUMO is a  $\pi$  bond delocalized over the adatom and the nitrogen atom (denoted  $\pi_{\text{AD=N}}^*$ ), while the LUMO+1 orbital is of  $\pi_{\text{C=N}}^*$  type [contained in the Si(111) plane].

As shown in Fig. 12, the calculated N 1s NEXAFS spectrum of the bridge<sub>N-AD</sub> plus broken PA-AD bond geometry presents two main transitions, one polarized orthogonal to the (111) plane, at 397.6 eV, and one polarized parallel to the (111) plane, at 398.0 eV. The former corresponds to a tran-

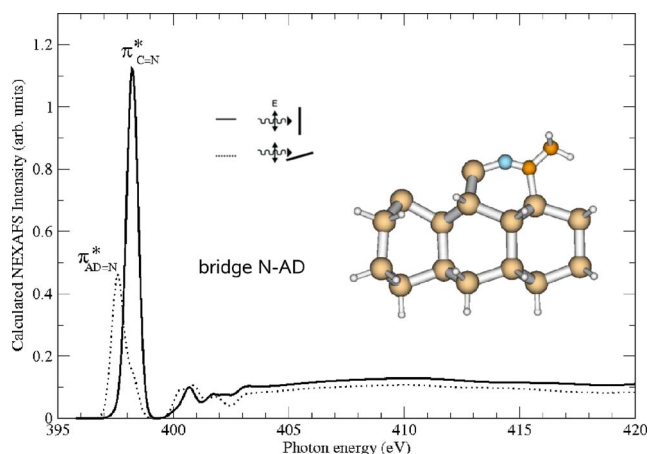


FIG. 12. (Color online) Simulated N 1s NEXAFS spectra of the bridge<sub>N-AD</sub> model (Si<sub>21</sub>H<sub>24</sub>, broken PA-AD bond), for two orientations of the electric field (solid line,  $\theta=90^\circ$ ; dotted line,  $\theta=20^\circ$ ). The threefold substrate symmetry is taken into account. The IP is 403.3 eV. The corresponding optimized geometry is given in the inset. Note the presence of a silicon-molecule mixed-state transition—denoted  $\pi^*_{AD=N}$ —at lower excitation energy than that of the  $\pi^*_{C=N}$  transition.

sition to the LUMO ( $\pi^*_{AD=N}$ ), while the latter corresponds to a transition to the LUMO+1 ( $\pi^*_{C=N}$ ). Therefore the energy ordering of the ground state is not modified. The energy splitting between these two main lines, as given by the  $(1s)^1(LUMO)^{1/2}(LUMO+1)^{1/2}$  method, is 0.4 eV (see Fig. 12), a value equal to that obtained from the  $\Delta$ KS energy difference (see Table III).

Finally we address the case of the “bridge<sub>N-RA</sub> plus broken PA-AD” model. The bridging of the molecule over the AD-RA site leads also, on a stiff rest plane, to the breaking of the PA<sub>1</sub>-AD bond, as shown in the inset of Fig. 13 (refer also to Table II). The total energy of this geometry is slightly larger (by 0.18 eV) than that of the “bridge<sub>N-AD</sub> plus broken PA-AD” model. The lower-energy transition is calculated at 397.4 eV, with a polarization normal to (111) (the related orbital, denoted “N 2p+Si db,” is mostly concentrated on the adatom dangling bond, but some weight is also distributed on the nitrogen). Note its intensity is much weaker than the  $\pi^*_{AD=N}$  transition of the N-AD model. The main calculated transition is the  $\pi^*_{C=N}$  transition at 398.1 eV, polarized in the (111) plane. Finally, the line at 399.5 eV—polarized normal to the surface—has a marked  $\sigma^*_{Si-N}$  character, similarly to the case of the “unbroken adatom backbond” N-RA geometry (Fig. 10).

#### 4. RA-cyanomethyl plus AD-H with a Si<sub>16</sub>H<sub>18</sub> cluster

We have optimized the dissociated geometry “RA-cyanomethyl plus AD-H” of Fig. 2(i), using the Si<sub>16</sub>H<sub>18</sub> cluster. The calculated CN bond length is 1.15 Å, a distance characteristic of a triple bond. The calculated NEXAFS spectra of RA-cyanomethyl are given in Fig. 14. The main  $\pi^*_{C=N}$  transition is calculated at 399.8 eV. As the threefold symmetry of the substrate is taken into account, the calculated  $\pi^*_{C=N}$  main transition is not dichroic.

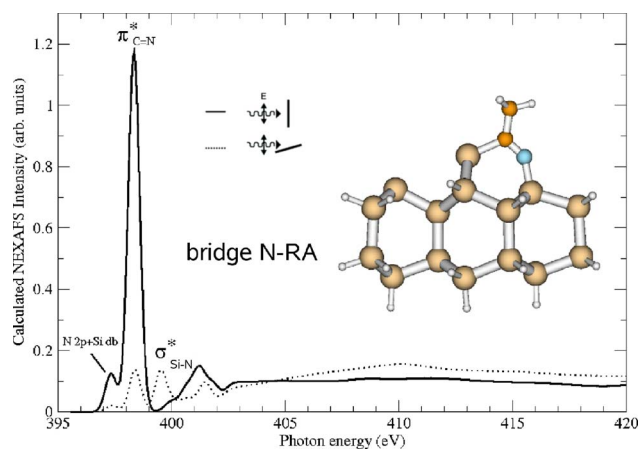


FIG. 13. (Color online) Simulated N 1s NEXAFS spectra of the bridge<sub>N-RA</sub> model (Si<sub>21</sub>H<sub>24</sub>), for two orientations of the electric field (solid line,  $\theta=90^\circ$ ; dotted line,  $\theta=20^\circ$ ). The threefold substrate symmetry is taken into account. Note the characteristic transition at 399.5 eV polarized perpendicularly to the (111) plane, associated with a Si-N axis close to the normal to the (111) plane. The IP is 402.98 eV. The corresponding optimized geometry is given in the inset. Note the dichroic behavior of the transitions to silicon-molecule mixed states, i.e., the “N 2p+Si db” line, which has most of its weight on the adatom dangling bond (db), and the  $\sigma^*_{Si-N}$  line.

#### C. Discussion of the adsorption models

NEXAFS calculations—reported in Table III—show that the geometries that bridge an AD-RA pair [they are depicted in Figs. 2(a)–2(d)] lead to  $\pi^*_{C=N}$  transitions in the 397.8–398.1 eV range, with a strong polarization in the (111) plane (i.e., the transition intensity is null at  $\theta=0^\circ$ ). The remarkable information provided by  $\Delta$ KS calculations is that the  $\pi^*_{C=N}$  transition energies depend little on the breaking or not of the adatom backbond. The lower  $h\nu$  experimental transition (at 397.65 eV) is therefore ascribed to a Si-C=N-Si unit.

On the other hand, it is clear that the intensity of the experimental  $\pi^*_{C=N}$  transition does not follow a  $\sin^2 \theta$  dependence at grazing incidence (see Fig. 7), as expected from a C=N unit with  $p$  lobes parallel to the surface plane. Indeed

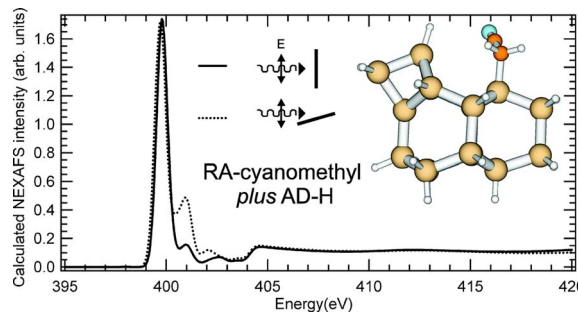


FIG. 14. (Color online) Simulated N 1s NEXAFS spectra of the “RA-cyanomethyl plus AD-H” model (Si<sub>16</sub>H<sub>18</sub> cluster), for two orientations of the electric field (solid line,  $\theta=90^\circ$ ; dotted line,  $\theta=20^\circ$ ). The threefold substrate symmetry is taken into account. The IP is 404.7 eV. The corresponding optimized geometry is given in the inset.

the experimental intensity at  $\theta=16^\circ$  is about  $\frac{1}{3}$  of the one at  $\theta=90^\circ$ . The apparent anomalous behavior of the  $\pi_{C\equiv N}^*$  transition at grazing incidence can be explained by the presence of electron transitions close in energy to the former. Those lines should correspond to transitions to molecular orbitals involved in the backbonding of the molecule. We already know (Sec. IV B) that their characteristic features (energy, dichroism) strongly depend on the type of bridging geometry.

Only “broken adatom backbond” bridge models give rise to calculated structures falling close to that of the  $\pi_{C\equiv N}^*$  (main) transition. In particular, the “broken PA-AD bond plus N-AD” model provides a strong silicon-nitrogen  $\pi^*$ -like state transition at 397.6 eV [polarized perpendicularly to the (111) plane], ca. 0.4 eV below the calculated  $\pi_{C\equiv N}^*$  transition (see Fig. 12 and Table III). Note that the width of the lower- $h\nu$  transition of Fig. 7 allows for the presence of two structures split by about 0.4 eV. Therefore the breaking of the adatom backbond cannot be excluded by our experimental data.

Now can we distinguish a  $\text{bridge}_{N-AD}$  bonding from a  $\text{bridge}_{N-RA}$  bonding? As indicated in Sec. IV B, NEXAFS transitions with a marked  $\sigma_{Si-N}^*$  character are obtained only in the case of the  $\text{bridge}_{N-RA}$  configuration. They are calculated 1.1 eV ( $\Delta$ KS calculation) above the  $\pi_{C\equiv N}^*$  transition for the unbroken adatom backbond model, and 1.4 eV [ $(1s)^1(\text{LUMO})^{1/2}(\text{LUMO}+1)^{1/2}$  calculation] for the broken adatom backbond model. They are polarized perpendicularly to the (111) plane. Such transitions should therefore appear at grazing incidence between the [(111)-polarized]  $\pi_{C\equiv N}^*$  and the (nondichroic)  $\pi_{C\equiv N}^*$  transitions. We note that no line at  $h\nu\sim 399$  eV is observed experimentally in the case of the acetonitrile-Si(111) system. On the other hand, in the case of the acetonitrile-Si(001) system, the theoretical NEXAFS spectrum of the Si-C $\equiv$ N-Si (end on) adsorption geometry exhibits a characteristic  $\sigma_{Si-N}^*$  transition at 399 eV, polarized perpendicularly to the surface plane (the angle between the Si-N axis and the surface normal is  $13^\circ$ ).<sup>28</sup> The experimental observation of a transition at  $h\nu=399$  eV, the energy predicted by theory for a  $\sigma_{Si-N}^*$  line, is the only feature that distinguishes the NEXAFS spectrum of the acetonitrile-Si(001) system from that of the acetonitrile-Si(111) one. Therefore, in the present case, the comparison of experiments vs theory favors the  $\text{bridge}_{N-AD}$  configuration over the  $\text{bridge}_{N-RA}$  one.

Concerning the dissociated species, the excited electronic states have only been calculated for the RA-cyanomethyl plus AD-H model. The calculated  $\pi_{C\equiv N}^*$  transition energy coincides with the transition observed experimentally at  $h\nu=399.8$  eV. Moreover we note also that the asymmetric shape of the experimental transition which increases at grazing incidence (see Fig. 7) is accounted for by the satellite calculated at 401 eV. The observed nondichroic behavior is also reproduced when the surface symmetry is taken into account. Consequently the experimental transition at 399.8 eV can be attributed to a cyanomethyl. However is the RA-cyanomethyl the only possible geometry? In fact, the AD-cyanomethyl plus RA-H geometry has an optimized geometry very similar to that of the RA-cyanomethyl plus

TABLE IV. Assignment of the experimental N 1s NEXAFS and XPS binding energies (given in eV) to adsorption models. FL is the Fermi level.

Experimental NEXAFS transitions	Experimental XPS binding energy with respect to FL	Assigned model
397.65	397.60	$\text{bridge}_{N-AD}$
399.80	398.95	AD-cyanomethyl or RA-cyanomethyl

AD-H [same CN bond length; about the same angle between the CN axis and the normal to the (111) plane]. We thus expect the same transition energies and dichroic behavior and therefore we have no practical means of distinguishing between those two adsorption geometries.

Our simulations indicate that all main experimental NEXAFS features are explained by the presence of Si-C $\equiv$ N-Si and free C $\equiv$ N blocks. This interpretation is coherent with the N1s XPS data and IP calculations. We note that the calculated IP energy difference between the bridge and cyanomethyl models is about 1.6 eV. This compares favorably with the experimental XPS binding energy shift of about 1.3 eV, measured between the two structures composing the spectrum of Fig. 6 (see also Table IV). Let us add that on the basis of XPS measurements, a C $\equiv$ N moiety datively bonded to a silicon is excluded, as its binding energy shift with respect to a C=N line should be larger than 3 eV,<sup>28</sup> which is not observed.

#### D. Adsorption mechanisms

As the confrontation of our experimental NEXAFS data with calculated spectra points to a N-AD bridge geometry, one could think of a reaction path in which the molecule approaches an “acidic” adatom site, forming a datively bonded precursor state via its nitrogen lone pair [Fig. 2(f)]. Therefore the charge transfer mechanism, where the electron charge of the “basic” rest atom is redirected toward its adatom neighbors, would not be at work here. If we follow the argument developed by Kang for NH<sub>3</sub> dissociation,<sup>12</sup> the formation of the datively bonded precursor state on the adatom would make it hypervalent (fivefold coordinated),<sup>49</sup> by which the backbond breaking would occur more readily.<sup>50</sup> In the case of acetylene adsorption, the DFT calculation of Sbraccia *et al.* shows (Fig. 4 of Ref. 27) a transition state in which the interaction of the molecule with the adatom (formation of Si-C bond) is accompanied by the breaking of the PA<sub>1</sub>-AD bond (indeed the  $\pi$  electrons of the molecule can be donated to the “acidic” adatom). Therefore, in the context of acetonitrile adsorption, PA<sub>1</sub>-AD bond breaking would occur before AD-RA bridging (mechanism 1 of Fig. 15). The possible reformation of the PA<sub>1</sub>-AD bond in a third step would not be likely, if we take into account our calculations using the “stiff” cluster indicating that the broken geometry is the only stable geometry, and periodic DFT calculations by Sbraccia *et al.* on the bridging geometry of acetylene.<sup>27</sup> Alternately (mechanism 2 of Fig. 15), one could imagine that the mo-

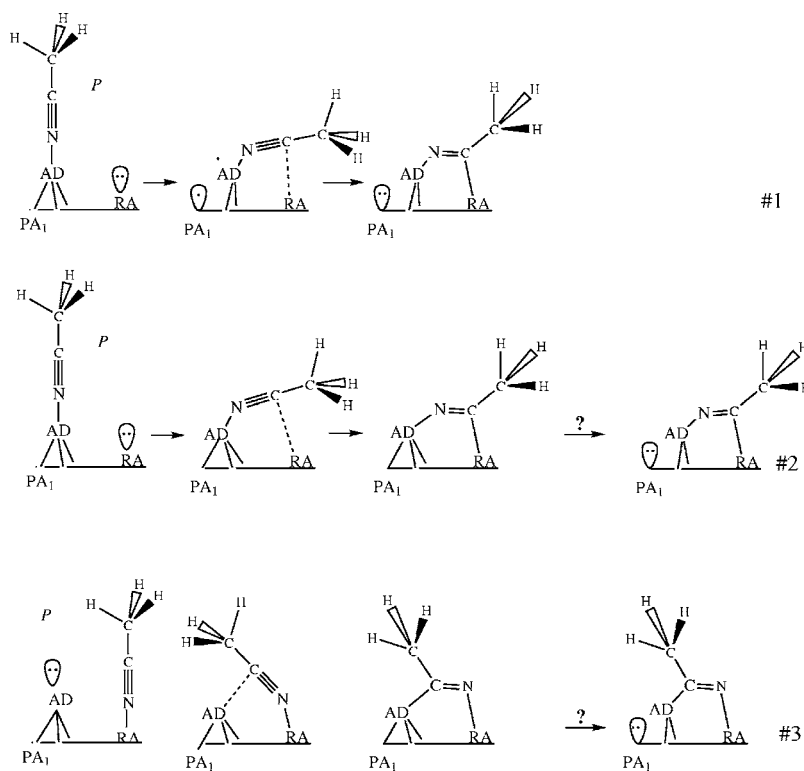


FIG. 15. Possible reaction paths leading to AD-RA bridging geometries. *P* is the molecular precursor, the acetonitrile molecule datively bonded to an adatom (or a rest atom) via its nitrogen lone pair. With respect to mechanisms 2 and 3, mechanism 1 is characterized by PA<sub>1</sub>-AD bond breaking before AD-RA bridging. In mechanisms 2 and 3, PA<sub>1</sub>-AD bond breaking after AD-RA bridging can be envisaged. Comparison of experimental NEXAFS spectra vs theoretical ones favors the N-AD bonding (i.e., the product resulting from mechanism 1 or 2) over the N-RA bonding (see Sec. IV C).

molecular precursor (without adatom destabilization) bends toward a nearby rest atom to form a bridge over the large adatom-rest atom pair site, maybe with a high activation barrier owing to the large bridging distance (4.5 Å). Bridging would be then followed by a possible breaking of the PA<sub>1</sub>-AD bond. Now if a precursor state forms on a rest atom site (mechanism 3), the rest atom, which becomes four-fold coordinated, is stabilized by the dative bonding in contrast with the adatom that was destabilized. Therefore for mechanism 3 as well, the AD-RA gap cannot be reduced, and a high activation barrier may exist because of the large bridging distance. Indeed, the experimental NEXAFS data favor the N-AD bonding.

As discussed before it is practically impossible to distinguish spectroscopically a RA-cyanomethyl from an AD-cyanomethyl. However in the absence of a charge transfer mechanism between rest atoms and adatoms, the acid-base reaction framework can be used to describe a reaction path. Assuming the same type of mechanism we proposed in Ref. 28 for C-H scission on Si(001), a proton could be transferred to the rest atom and simultaneously the CH<sub>2</sub>CN<sup>-</sup> unit could bond via its C lone pair to the adatom to form an AD-cyanomethyl.

V. CONCLUDING REMARKS

Bearing a lone pair on its nitrogen end (like ammonia) and being a π-bonded molecule (like the alkenes and the alkynes) the acetonitrile molecule, when deposited on the Si(111)-7×7 surface, appears as a probe molecule capable of unveiling some interesting aspects of the surface electronic structure (acidic and basic sites, possible charge trans-

fer phenomena between surface states, lability of the adatoms).

Combining N 1s core-level spectroscopies with DFT electronic transition calculations, we have determined the electronic structure of acetonitrile chemisorbed at 300 K. Two chemical states for the molecule are identified, corresponding to a -C≡N- unit (NEXAFS transition at hν = 397.65 eV) and a pendent C=N unit (NEXAFS transition at hν = 399.8 eV). Thus the state of things is different from that studied at 110 K, for which HREELS spectroscopy detected only the sp-to-sp<sup>2</sup> re-hybridization.<sup>22</sup> Datively bonded geometries are excluded at 300 K by our NEXAFS and XPS experimental data. However, they may play a key role as precursors to the observed geometries.

Our N 1s NEXAFS simulation of the Si-C=N-Si adsorption modes, which bridge adjacent adatom-rest atom pairs, used two types of clusters, a “flexible” Si<sub>16</sub>H<sub>18</sub> cluster and a “rigid rest plane” Si<sub>21</sub>H<sub>24</sub> cluster. Upon adatom-rest atom bridging, the pedestal atom-adatom bond breaks in the case of the stiff cluster, while this is avoided in the case of the flexible one. However, for both clusters, molecular bridging induces about the same strong reduction of the adatom-rest atom distance. While calculations predict a σ<sub>Si-N</sub><sup>\*</sup> NEXAFS transition [polarized perpendicular to the (111) plane] at 399-399.5 eV only in the case when nitrogen is bonded to the rest atom, its absence in the experimental spectrum lends more support to an attachment of the nitrogen end to the adatom. A selective attachment on the adatom may proceed from a datively bonded precursor (via donation of its N lone pair to the adatom dangling bond), and therefore the rest atom-adatom charge transfer scheme<sup>5</sup> would not be at work for acetonitrile. Let us add that for the bridge N-AD geometry, the breaking of the pedestal-adatom bond has a strong

effect on the calculated N1s NEXAFS spectra (a  $\pi$ -type bond delocalized over the nitrogen atom and the adatom appears): this may explain the apparent dichroic behavior of the experimental  $\pi_{C=N}^*$  transition at  $h\nu=397.65$  eV.

To account for the presence of a free (nondatively bonded) C $\equiv$ N group, we propose that the molecule can also dissociate on the surface, to give a cyanomethyl unit (Si-CH<sub>2</sub>C $\equiv$ N) plus a silicon monohydride. This model is suggested by the acidic nature of the methyl hydrogens. The corresponding calculated N 1s NEXAFS energy coincides with the experimental one. However the present spectroscopic information does not enable us to distinguish between an attachment of the cyanomethyl to the adatom or to the rest atom.

We can note also that the reactivity of acetonitrile on Si(111)-7 $\times$ 7 and Si(001)-2 $\times$ 1 is very similar, leading in both cases to the formation of  $sp^2$  adducts and to the breaking of the C-H bond (formation of a cyanomethyl). Because the minimal distances between pairs of surface silicon dangling bonds are very different on Si(111) (4.5 Å) and Si(001) (2.35 Å), this observation is puzzling, but is not isolated. Indeed alkenes, alkynes, water, and ammonia tend to react the same way on both surfaces. All these molecules possess a common feature: they can form a dative bond (via the  $\pi$  electrons or the oxygen-nitrogen lone pair) with the adatom. Therefore the possible lability of the adatom due to the dative bond of an adsorbed molecule, first discussed theoretically by Kang for ammonia,<sup>12</sup> can explain why the same products are observed on both surfaces, as the breaking of the pedestal atom-adatom bond reduces the adatom-restatom distance to 3.4–3.6 Å.

On the other hand the two surfaces differ by the role played by their gap states in the positioning of the Fermi level. While the Fermi level moves up in the gap by about 140 meV after molecular adsorption in the case of the (001)-2 $\times$ 1 surface,<sup>51</sup> for the (111)-7 $\times$ 7 surface it remains pinned at the same position within the gap. All surface states are quenched on Si(001), while some remain on Si(111) even after surface saturation (e.g., at saturation coverage, adatoms are still observed<sup>22</sup> by STM), or new ones may be created (e.g., due to a possible pedestal atom-adatom bond breaking, as shown in Fig. 11).

Further experimental work is needed to better understand the reactivity of acetonitrile on this complex surface. Detailed kinetic studies combining various surface science techniques (spectroscopical tools and STM) would be useful, to determine, for instance, the formation rate of the various species vs exposure, and to obtain a quantitative value of the saturation coverage. A detailed scanning tunneling spectroscopy study over the adatom sites should give information on the possible breaking of the pedestal atom-adatom bond, and the correlated possible formation of “double bridge” adducts. It is indeed clear that the question of the lability of the adatom—destabilized by a dative bonding—is of particular interest, because of its general applicability in the determination of the reaction paths of many molecules. We hope that the present core-level spectroscopy study will also stimulate theoretical works in this direction.

#### ACKNOWLEDGMENTS

We are grateful for a generous allocation of computational time in the IBM RS/6000SP machine of IDRIS/CNRS.

\*Electronic address: carniato@ccr.jussieu.fr

<sup>†</sup>Present address: Rutgers University, Department of Physics and Astronomy, 136 Frelinghuysen Road, Piscataway, NJ 08854, USA. Email address: rangan@physics.rutgers.edu

<sup>‡</sup>Electronic address: roch@ccr.jussieu.fr

- <sup>1</sup>M. Filler and S. Bent, *Prog. Surf. Sci.* **73**, 1 (2003).
- <sup>2</sup>K. Takayanagi, Y. Tanishiro, M. Takahashi, and S. Takahashi, *J. Vac. Sci. Technol. A* **3**, 1502 (1985).
- <sup>3</sup>R. Losio, K. N. Altmann, and F. J. Himpsel, *Phys. Rev. B* **61**, 10845 (2000).
- <sup>4</sup>R. Wolkow and P. Avouris, *Phys. Rev. Lett.* **60**, 1049 (1988).
- <sup>5</sup>P. Avouris and R. Wolkow, *Phys. Rev. B* **39**, 5091 (1989).
- <sup>6</sup>R. M. Tromp, R. J. Hamers, and J. E. Demuth, *Phys. Rev. B* **34**, 1388 (1986).
- <sup>7</sup>F. J. Himpsel and T. Fauster, *J. Vac. Sci. Technol. A* **2**, 1984 (1984).
- <sup>8</sup>S. Tong, H. Huang, C. M. Wei, W. Packard, F. Men, G. Glander, and M. Webb, *J. Vac. Sci. Technol. A* **6**, 615 (1988).
- <sup>9</sup>R. J. Hamers, R. M. Tromp, and J. E. Demuth, *Phys. Rev. Lett.* **56**, 1972 (1986).
- <sup>10</sup>T. Uchihashi, Y. Sugawara, T. Tsukamoto, M. Ohta, S. Morita, and M. Suzuki, *Phys. Rev. B* **56**, 9834 (1997).
- <sup>11</sup>X. Lu, X. Xu, N. Wang, Q. Zhang, and M. C. Lin, *Chem. Phys. Lett.* **355**, 365 (2002).

- <sup>12</sup>M.-H. Kang, *Phys. Rev. B* **68**, 205307 (2003).
- <sup>13</sup>J. M. Buriak, *Chem. Rev. (Washington, D.C.)* **102**, 1272 (2002).
- <sup>14</sup>R. Wolkow, *Annu. Rev. Phys. Chem.* **50**, 413 (1999).
- <sup>15</sup>J. Yoshinobu, H. Tsuda, M. Onchi, and M. Nishijima, *Chem. Phys. Lett.* **30**, 170 (1986).
- <sup>16</sup>F. Rochet, G. Dufour, P. Prieto, F. Sirotti, and F. C. Stedile, *Phys. Rev. B* **57**, 6738 (1998).
- <sup>17</sup>V. De Renzi, R. Biagi, and U. del Pennino, *Phys. Rev. B* **64**, 155305 (2001).
- <sup>18</sup>J. Yoshinobu, H. Tsuda, M. Onchi, and M. Nishijima, *Solid State Commun.* **60**, 801 (1986).
- <sup>19</sup>M. N. Piancastelli, N. Motta, A. Sgarlata, A. Balzarotti, and M. De Crescenzi, *Phys. Rev. B* **48**, 17892 (1993).
- <sup>20</sup>F. Rochet, F. Jolly, F. Bournel, G. Dufour, F. Sirotti, and J. L. Cantin, *Phys. Rev. B* **58**, 11029 (1998).
- <sup>21</sup>N. Shirota, S. Yagi, M. Taniguchi, and E. Hashimoto, *J. Vac. Sci. Technol. A* **18**, 2578 (2000).
- <sup>22</sup>F. Tao, X. F. Chen, Z. H. Wang, and G. Q. Xu, *J. Phys. Chem. B* **106**, 3890 (2002).
- <sup>23</sup>F. Tao and G. Q. Xu, *Phys. Rev. B* **66**, 035420 (2002).
- <sup>24</sup>F. Tao, Z. H. Wang, X. F. Chen, and G. Q. Xu, *Phys. Rev. B* **65**, 115311 (2002).
- <sup>25</sup>M. Carbone, G. Comtet, G. Dujardin, L. Hellner, and A. J. Mayne, *J. Chem. Phys.* **117**, 5012 (2002).

- <sup>26</sup>X. Lu, X. Wang, Q. Yuan, and Q. Zhang, *J. Am. Chem. Soc.* **125**, 7923 (2003).
- <sup>27</sup>C. Sbraccia, C. A. Pignedoli, A. Catellani, R. di Felice, P. L. Silvestri, F. Toigo, F. Ancilotto, and C. M. Bertoni, *Surf. Sci.* **557**, 80 (2004).
- <sup>28</sup>S. Rangan, F. Bournel, J.-J. Gallet, S. Kubsky, K. Le Guen, G. Dufour, F. Rochet, F. Sirotti, S. Carniato, and V. Ilakovac, *Phys. Rev. B* **71**, 165319 (2005).
- <sup>29</sup>In  $\text{CH}_3\text{-C}\equiv\text{N}$ , donation of a pseudo- $\pi$ -orbital on the methyl group to the  $\pi$  orbital of the triple bond weakens the C-H bond. See P. M. Mayer, M. S. Taylor, M. W. Wong, and L. Radom, *J. Phys. Chem. A* **102**, 7074 (1998).
- <sup>30</sup>C. Poncey, F. Rochet, G. Dufour, H. Roulet, F. Sirotti, and G. Panaccione, *Surf. Sci.* **338**, 143 (1995).
- <sup>31</sup>F. Jolly, F. Rochet, G. Dufour, C. Grupp, and A. Taleb-Ibrahimi, *J. Non-Cryst. Solids* **280**, 150 (2001).
- <sup>32</sup>G. Dufour, F. Rochet, H. Roulet, and F. Sirotti, *Surf. Sci.* **304**, 33 (1994).
- <sup>33</sup>S. Rangan, J.-J. Gallet, F. Bournel, S. Kubsky, K. Le Guen, G. Dufour, F. Rochet, F. Sirotti, S. Carniato, and V. Ilakovac, *Phys. Rev. B* **71**, 165318 (2005).
- <sup>34</sup>F. Sirotti, F. Polack, J. Cantin, M. Sacchi, R. Delaunay, M. Meyer, and M. Liberati, *J. Synchrotron Radiat.* **7**, 5 (2000).
- <sup>35</sup>F. Rochet, C. Poncey, G. Dufour, H. Roulet, W. N. Rodrigues, M. Sauvage, J. C. Bouliard, F. Sirotti, and G. Panaccione, *Surf. Sci.* **326**, 229 (1995).
- <sup>36</sup>J. Stöhr, *NEXAFS Spectroscopy* (Springer, Berlin, 1992).
- <sup>37</sup><http://www.msg.ameslab.gov/GAMESS/GAMESS.html>
- <sup>38</sup>S. Carniato, V. Ilakovac, J. J. Gallet, E. Kukuk, and Y. Luo, *Phys. Rev. A* **70**, 032510 (2004).
- <sup>39</sup>W. Kutzelnig, U. Fleisher, and M. Schindler, *Chemical Shifts and Magnetic Susceptibilities* (Springer, Berlin, 1990), Vol. 23.
- <sup>40</sup>L. Triguero, O. Plashkevych, L. G. M. Pettersson, and H. Agren, *J. Electron Spectrosc. Relat. Phenom.* **104**, 195 (1999).
- <sup>41</sup>T. Ziegler, A. Rauk, and E. J. Baerends, *Theor. Chim. Acta* **43**, 261 (1977).
- <sup>42</sup>A. Hitchcock, M. Tronc, and A. Modelli, *J. Phys. Chem.* **93**, 3068 (1989).
- <sup>43</sup>D. Beach, C. Eyermann, S. Smit, S. Xiang, and W. Jolly, *J. Am. Chem. Soc.* **106**, 536 (1984).
- <sup>44</sup>S. Carniato, V. Ilakovac, J.-J. Gallet, E. Kukuk, and Y. Luo, *Phys. Rev. A* **71**, 022511 (2005).
- <sup>45</sup>J. Stöhr, *NEXAFS Spectroscopy* (Ref. 36), p. 233.
- <sup>46</sup>P. W. Langhoff, *Chem. Phys. Lett.* **22**, 60 (1973).
- <sup>47</sup>F. J. Himpsel, B. S. Meyerson, F. R. McFeely, J. F. Morar, A. Taleb-Ibrahimi, and J. A. Yarmoff, in *Photoemission and Photoabsorption Spectroscopy of Solids and Interfaces with Synchrotron Radiation, Proceedings of the International School of Physics "Enrico Fermi,"* edited by M. Campagna and R. Rosei, (North-Holland, Amsterdam, 1990), p. 203.
- <sup>48</sup>F. J. Himpsel, G. Hollinger, and R. A. Pollak, *Phys. Rev. B* **28**, 7014 (1983).
- <sup>49</sup>In fact, the adatom forms three bonds with the three pedestal atoms, and a (weak) fourth one with a silicon right below it (see Fig. 1 and Ref. 5 of the present paper).
- <sup>50</sup>To break the adatom backbond a calculated activation energy of 0.8 eV has to be overcome [K. Cho, E. Kaxiras, and J. D. Joannopoulos, *Phys. Rev. Lett.* **79**, 5078 (1997)]. Apparently, a dative bonding greatly reduces the barrier height.
- <sup>51</sup>F. Bournel, J.-J. Gallet, S. Kubsky, G. Dufour, F. Rochet, M. Simeoni, and F. Sirotti, *Surf. Sci.* **513**, 37 (2002).